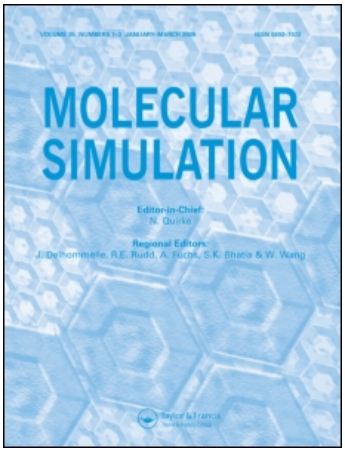

Molecular Simulation
Publication details, including instructions for authors and subscription information:
http://www.informaworld.com/smpp/title~content=t713644482

Molecular simulation study of the quantum effects of hydrogen adsorption in metal-organic frameworks: influences of pore size and temperature

Qing Xu[a]; Dahuan Liu[a]; Qingyuan Yang[a]; Chongli Zhong[a]
[a] Laboratory of Computational Chemistry, Department of Chemical Engineering, Beijing University of Chemical Technology, Beijing, P.R. China

To cite this Article Xu, Qing , Liu, Dahuan , Yang, Qingyuan and Zhong, Chongli(2009) 'Molecular simulation study of the quantum effects of hydrogen adsorption in metal-organic frameworks: influences of pore size and temperature', Molecular Simulation, 35: 9, 748 — 754
To link to this Article: DOI: 10.1080/08927020902824839
URL: http://dx.doi.org/10.1080/08927020902824839

Molecular Simulation
Vol. 35, No. 9, August 2009, 748–754

Taylor & Francis
Taylor & Francis Group

Molecular simulation study of the quantum effects of hydrogen adsorption in metal-organic frameworks: influences of pore size and temperature

Qing Xu, Dahuan Liu, Qingyuan Yang* and Chongli Zhong

Laboratory of Computational Chemistry, Department of Chemical Engineering, Beijing University of Chemical Technology, Beijing 100029, P.R. China

(*Received 16 December 2008; final version received 14 February 2009*)

In this work a systematic molecular simulation study was performed to investigate the influence of pore size and temperature on the quantum effects of hydrogen adsorption in metal-organic frameworks (MOFs) with temperature varied from 40 to 120 K. To do this, three isoreticular MOFs (IRMOFs) with different pore sizes were adopted, and quadratic Feynman–Hibbs (FH) effective potential was introduced to consider the quantum effect. The results show that quantum effects diminish with increasing pore size of IRMOFs at lower pressure (loading), while the opposite trend appears at higher pressure (loading). Through the simulations it is also found that the quantum effects may be dominantly determined by the adsorbate–adsorbate or adsorbate–MOFs interactions with the varying of pressure (loading). In addition, the results also indicate how the temperature influences the quantum effects of H_2 adsorption in MOFs within the pressure range considered.

Keywords: molecular simulation; quantum effects; hydrogen adsorption; metal-organic frameworks

1. Introduction

Hydrogen has received much attention as an alternative replacement for fossil fuels in mobile applications because of its clean combustion and high-heating value. A safe and efficient storage system is crucial for the future wide utilisation of hydrogen in vehicles and portable electronics. Although various materials have been studied as hydrogen storage materials, no suitable material can meet the US Department of Energy (DOE) cost and performance targets yet. Among the subset of highly porous materials, metal-organic frameworks (MOFs) are thought to be a set of promising hydrogen storage materials [1–5]. Various MOFs have been synthesised and characterised for their hydrogen storage capacities [6–11], some of which get close to the DOE targets. These materials have an advantage over the traditional porous materials, such as zeolites and activated carbons, primarily due to their adjustable chemical functionality and fine-tunable pore structures. However, since quantum effects have been found to be important in the amount of H_2 adsorbed in these traditional porous materials [12–26], more and more attention has been paid to these effects in MOFs [27–32]. For example, Garberoglio et al. [27] indicated that quantum effects reduce the amount of H_2 adsorbed in isoreticular MOF (IRMOF)-1 and IRMOF-8 at 77 K, and also carried out quantum mechanical calculations for the selectivity of hydrogen isotopes in various organic frameworks [28]. Liu et al. [29,30] showed that it was critical to account for quantum effects of H_2 for both adsorption and diffusion in MOFs at low temperature. Noguchi et al. [31] found that the quantum-simulated H_2 and D_2 isotherms at 77 K using the FH effective potential coincided with the experimental ones, giving direct evidence on the quantum molecular sieving effect for the H_2 and D_2 adsorption in CuBOTf. Chen et al. [32] showed that quantum effects influence diffusion of H_2 and D_2 in the pores of M'MOF1 through the experimental method.

Few studies, however, have illuminated how the pore size and temperature influence the quantum effects of H_2 adsorption up to now. Since quantum effects can result from both adsorbate–adsorbate and adsorbate–adsorbent interactions, it is very difficult to study experimentally how these two interactions affect the adsorption behaviours under different loadings. Thus, in this work a systematic grand canonical Monte Carlo (GCMC) simulation was conducted to study the H_2 adsorption in MOFs. The results will exhibit the relationship between the pore size and temperature with the quantum effects of hydrogen adsorption in MOF materials.

2. Computational details

2.1 MOF structures

In this work, three typical IRMOFs (IRMOFs-1, -10, and -11) synthesised by Eddaoudi et al. [33] were selected, and their structures were constructed from their X-ray diffraction (XRD) data [33] using Materials Studio® Visualizer [34], as shown in Figure 1. These IRMOFs

*Corresponding author. Email: qyyang@mail.buct.edu.cn

ISSN 0892-7022 print/ISSN 1029-0435 online

DOI: 10.1080/08927020902824839
http://www.informaworld.com

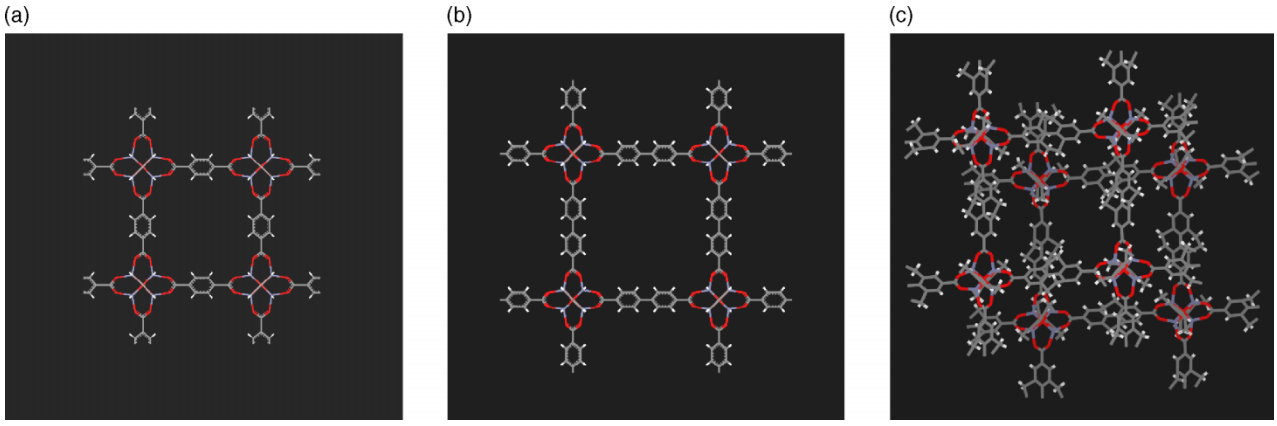

Figure 1. Crystal structures of the IRMOFs used in the simulation: (a) IRMOF-1, (b) IRMOF-10, (c) IRMOF-11 (Zn, blue; O, red; C, grey, and H, white).

feature the same primitive cubic topology with the octahedral $Zn_4O(CO_2)$ clusters linked by different organic dicarboxylate linkers. They have different pore sizes, and the size order is IRMOF-11 < IRMOF-1 < IRMOF-10 (see Table 1). The structural properties [33,35] for these IRMOF materials are summarised in Table 1, where the free volumes were calculated using a probe size of 0.0 Å to determine the total free volume not occupied by the framework atoms.

2.2 *Force fields*

Force fields play an important role in molecular simulations. In this study, H_2 was treated as a diatomic molecule, which was modelled by a Lennard-Jones (LJ) core located at its centre of mass and three partial charges with two ($q = 0.468e$) located at H atoms and one ($q = -0.936e$) at the centre between two H atoms. The bond length between two H atoms is 0.74 Å. The adopted LJ parameters for H_2 molecule were suggested by Marx and Nielaba [36] and are shown in Table 2. Such potential model has been successfully adopted to predict the adsorption of hydrogen in carbon nanohorns [24] and MOFs [37,38].

An atomistic representation was used to model all of the IRMOFs studied here. A combination of the site–site LJ and Coulombic potentials was used to calculate the interactions between adsorbate molecules and adsorbents. The LJ parameters for the framework atoms in IRMOFs were adopted from the universal force field of Rappé et al. [39], which has been successfully employed to depict the adsorption of several light gases and their mixtures in MOFs [27,40–42]. The potential parameters used in this work are listed in Table 2. The partial charges for the atoms in IRMOF-1 and IRMOF-10 were taken from our previous work [43], which was obtained from the density functional theory calculations combined with unrestricted B3LYP functional and ChelpG method. Since the atomic partial charges are mainly determined by the chemical bonds among atoms, it is thought that the atomic partial charges in IRMOF-11 can be transferred from its corresponding counterpart IRMOF-12 [43]. In our simulations, all the LJ cross-interaction parameters were determined by the Lorentz–Berthelot mixing rules.

To take into account the quantum effects, the quadratic FH effective potential [44,45] was adopted to calculate all of the LJ interactions,

$$U_{\mathrm{FH}} = U_{\mathrm{LJ}}(r) + \frac{\hbar^2}{24\mu k_{\mathrm{B}}T}\left[U''_{\mathrm{LJ}}(r) + \frac{2U'_{\mathrm{LJ}}(r)}{r}\right], \quad (1)$$

where U_{LJ} denotes the classical LJ potential, r is the molecule–molecule distance, $\hbar$ is Planck's constant divided by 2π; the prime and double prime denote the first and second derivatives with respect to r, respectively. The second term in Equation (1) is the quantum correction,

Table 1. Structural properties of the MOFs studied in this work.

Material	Pore shape[a]	Unit cell (Å)	Cell angle (°)	d_{pore}[b] (Å)	ρ_{crys}[a] (g/cm^3)	V_{free}[c] (cm^3/g)
IRMOF-1	Cubic	$a = b = c = 25.832$	$\alpha = \beta = \gamma = 90$	10.9/14.3	0.59	1.36
IRMOF-10	Cubic	$a = b = c = 34.2807$	$\alpha = \beta = \gamma = 90$	16.7/20.2	0.33	2.66
IRMOF-11	Cubic/ catenation	$a = b = 24.8217$, $c = 56.7340$	$\alpha = \beta = 90$, $\gamma = 120$	3.5/3.8/4.7/ 6.1/7.3/11.1	0.76	0.92

[a] Obtained from the XRD crystal data [33]. [b] Obtained from the literature [35]. [c] Calculated with the Materials Studio package.

Table 2. LJ potential parameters for H_2 and the IRMOFs used in this work.

LJ parameters	H_2	MOF_O	MOF_C	MOF_H	MOF_Zn
σ (Å)	2.958	3.12	3.43	2.57	2.46
ε/k_B (K)	36.7	30.19	52.84	22.14	62.40

the parameter μ is the reduced mass, $\mu = m/2$ for H_2–H_2 interaction, and $\mu = m$ for H_2–adsorbent, where m is mass of H_2 molecule.

2.3 *Simulation method*

GCMC simulations were used to study H_2 adsorption in IRMOFs. Details on the method can be found elsewhere [46]. Modified Benedict–Webb–Rubin equation of state [47] for H_2 was used to relate the bulk pressure with fugacity required in the GCMC simulations. Similar to previous works [37,38,40–43,48,49], all the IRMOFs were treated as rigid frameworks, with atoms frozen at their crystallographic positions during simulations. The simulation box representing IRMOFs contained 8 ($2 \times 2 \times 2$) unit cells. The simulations with larger boxes showed that no finite-size effects existed using the above boxes. A cut-off radius of 13.0 Å was applied to all the LJ interactions, and the long-range electrostatic interactions were handled using the Ewald summation technique. Periodic boundary conditions were applied in all three dimensions. Since the adsorbent was assumed to be a rigid structure, the potential energies between an adsorbate and the adsorbent were initially tabulated on a series of three dimensional grid points with grid spacing 0.15 Å. During the simulations, the potential energy at any position in the adsorbent was determined by interpolation [27,37,38,43]. For each state point, GCMC simulation consisted of 1.5×10^7 steps to guarantee the equilibration, followed by 1.5×10^7 steps to sample the desired thermodynamic properties.

3. Results and discussion

3.1 *Validation of the force field*

To further confirm the reliability of the force field adopted in this work, the bulk PVT properties of H_2 in the temperature range of 40–120 K were calculated by NPT-MC simulations with the FH effective potential as well as classical LJ potential. Compared with experimental data [50], the results shown in Figure 1(a) evidently indicate that the PVT properties of H_2 are accurately reproduced by the FH effective potential over the whole pressure and temperature ranges considered in this work. Furthermore, GCMC simulations were also performed to calculate the adsorption isotherm of pure H_2 in IRMOF-1 at 77 K. The results in Figure 2(b) show that the simulations achieve good reproduction of the experimental adsorption isotherm of H_2 [11]. Therefore, the force fields adopted in this work are reliable to investigate the adsorption behaviours of H_2 in IRMOFs.

3.2 *Influence of pore size*

In order to investigate how pore size influences the quantum effects of H_2 adsorption in MOFs, a series of GCMC simulations were carried out in two cases, i.e. classical simulations without considering all of the quantum effects (case 1), and those considering all of the quantum effects (case 2). The contribution values of the quantum effects of H_2 adsorption in three IRMOFs (denoted as $V_{contribution}$) were calculated by Equation (2) at five different temperatures, and

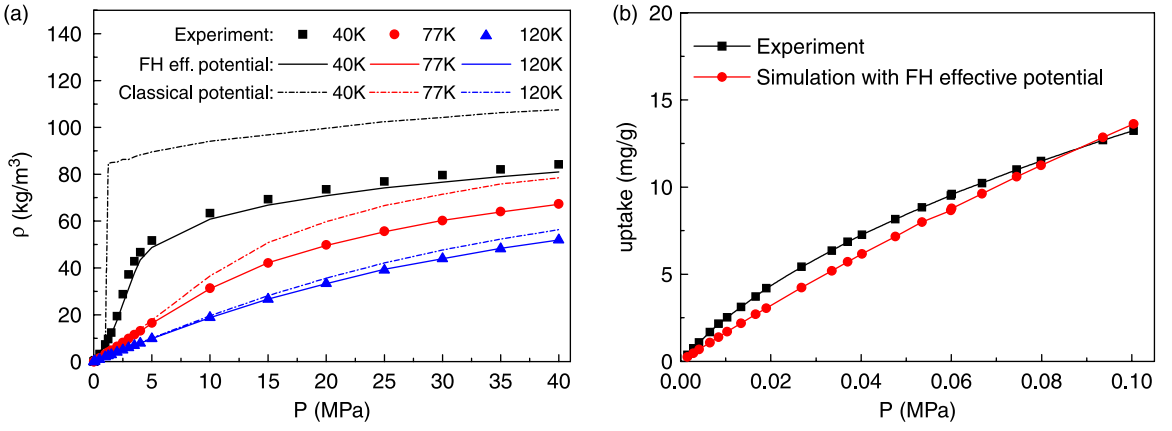

Figure 2. Comparison of simulated and experimental results: (a) PVT properties of bulk H_2 with temperature varied from 40 to 120 K; (b) adsorption isotherms of H_2 in IRMOF-1 at 77 K.

the results are shown in Figure 3

$$V_{\text{contribution}} = -\frac{N_{\text{ads}}^{\text{qm}} - N_{\text{ads}}^{\text{no}}}{N_{\text{ads}}^{\text{no}}} \times 100\%, \qquad (2)$$

where $N_{\text{ads}}^{\text{no}}$ and $N_{\text{ads}}^{\text{qm}}$ are the adsorbed amounts in cases 1 and 2, respectively.

As can be seen from Figure 3, at very low pressure, the $V_{\text{contribution}}$ in IRMOF-11 is the largest among the three IRMOFs considered in this work, which indicates the quantum effects of H_2 adsorption in IRMOFs with smaller pore size (see Table 1) are more evident. This observation can be explained by the following: the adsorb molecules are few at very low pressure, and much smaller pores in IRMOF-11 leads to stronger quantum effects due to the space confinement. With the pressure increasing, the quantum effects of H_2 adsorption in these IRMOFs becomes weaker. In addition, at higher pressures, the values of $V_{\text{contribution}}$ in IRMOFs-1, -10, and -11 have the order IRMOF-11 < IRMOF-1 < IRMOF-10, which is consistent with

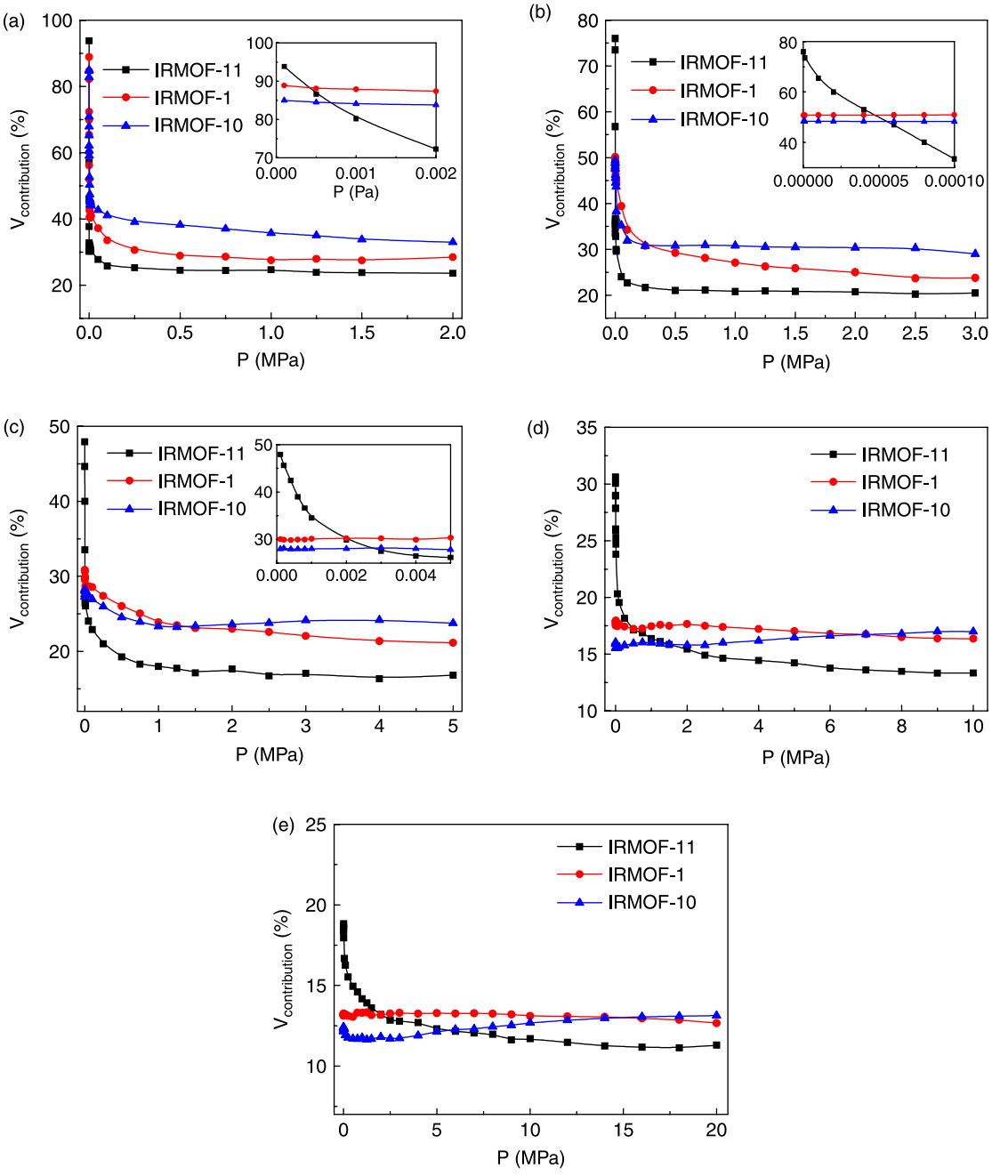

Figure 3. Comparison of the contribution values of quantum effects of H_2 adsorption in three IRMOFs with various temperatures: (a) 40, (b) 60, (c) 77, (d) 100, (e) 120 K. The results at low pressure are shown in the inset for clear.

gradually increasing sequence of pore size (see Table 1). This indicates that the quantum effects of H_2 adsorption in IRMOFs with large pore size are more evident at relative high pressure. Detailed discussions on this reverse trend will be given in the next part. Furthermore, the $V_{contribution}$–pressure curves for IRMOF-11 with various small pores contain two steps: a quick decrease at low pressures, followed by a slow decrease with further increasing pressure, and this trend becomes more pronounced with decreasing temperature. Similar phenomena were also found in IRMOF-1 and IRMOF -10 with large pore size below 77 K, but the changes of $V_{contribution}$ are not significant with increasing temperature. Thus, we can draw a conclusion that, at low pressure (loading), the smaller the pore size, the more evident the quantum effects; while at high pressure (loading) an opposite result appears.

3.3 Influence of quantum effects for various intermolecular interactions

To further understand whether the above observations resulted from the quantum effects for adsorbate–adsorbate interactions or adsorbate–IRMOFs interactions, two additional GCMC simulations were performed for H_2 adsorption in IRMOFs: case 3, switching off the quantum effects for adsorbate–adsorbate interactions, and case 4, switching off the quantum effects for adsorbate–IRMOFs interactions. Then the contribution values of the quantum effects for various kinds of interaction were also calculated by Equation (2). Here, N_{ads}^{no} is also calculated from the case 1, but N_{ads}^{qm} could be N_{ads}^{fm} which is calculated from the case 3 or N_{ads}^{ff} which is calculated from the case 4. Since the results at different temperatures are similar, only the results at 60 K are shown in Figure 4, together with the results in case 2 (considering all of the quantum effects), included for comparison.

From this figure, it is evident that the contributions of quantum effects for various intermolecular interactions depend on the pressure. At very low pressures, the amount of molecules adsorbed in the materials is very small, and the influence of the quantum effects for interactions between adsorbed molecules is negligible, which can explain the identical contribution value in cases 2 and 3. It can also be found in Figure 4 that the contributions of the quantum effects for adsorbate–IRMOFs interactions are much higher than those between adsorbate molecules

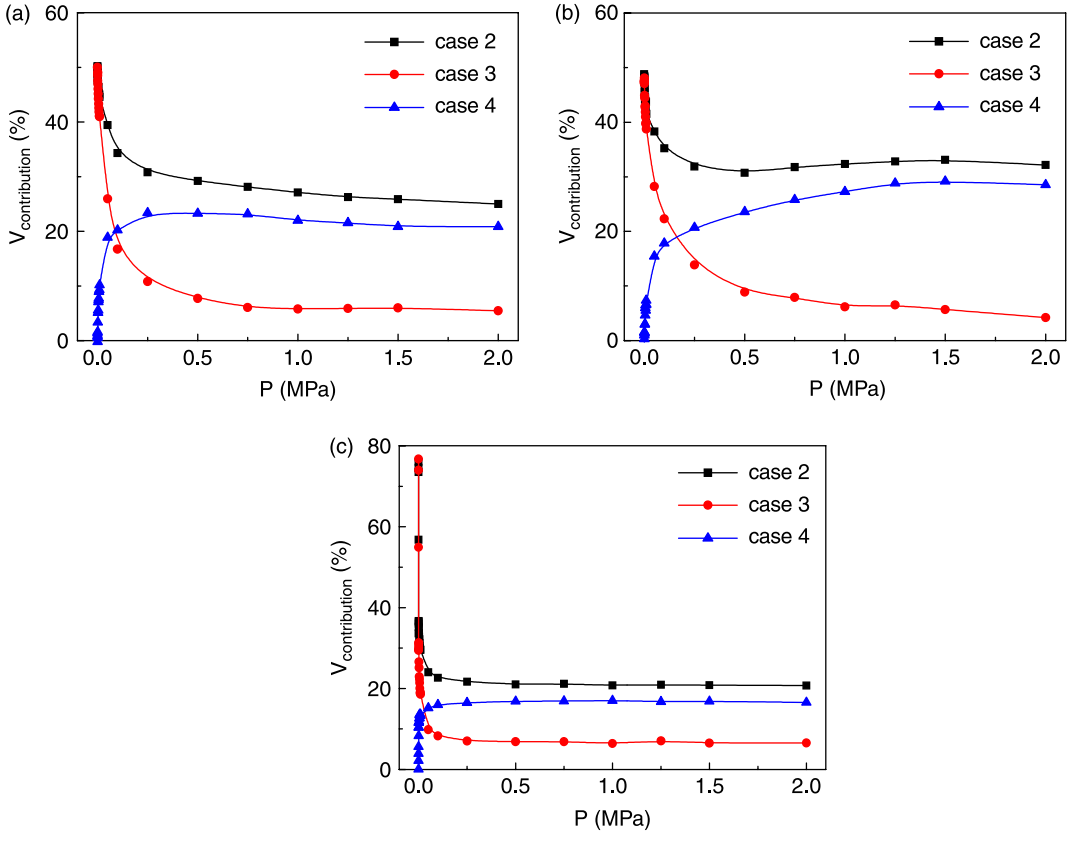

Figure 4. Comparison of quantum effects for various interactions of H_2 adsorption in three IRMOFs at 60 K: (a) IRMOF-1, (b) IRMOF-10, (c) IRMOF-11; case 2: considering all of the quantum effects; case 3: switching off the quantum effects for adsorbate–adsorbate interactions; case 4: switching off the quantum effects for adsorbate–IRMOFs interactions.

at low pressure (loading), which indicates that the quantum effects mainly depend on the interactions between adsorbate and IRMOFs. With the pressure increasing, the quantum effects principally result from the adsorbate–adsorbate interactions. At low pressure, IRMOFs with small pore size can adsorb more molecules easily; thus, the contribution of the quantum effects for the interactions between adsorbate and IRMOF-11 is the strongest among these three IRMOFs. While at high pressure, due to the fact that IRMOFs with large pore size can accommodate more H_2 molecules, the quantum effects resulting from adsorbate–adsorbate interactions are more evident in IRMOF-1 and IRMOF-10. That is why the contributions of quantum effects of H_2 adsorption in MOFs show different dependence on the pore size with the varying of pressure.

3.4 Influence of temperature

To investigate how the temperature influences the quantum effects of H_2 adsorption in MOF materials, a series of GCMC simulations was further performed on H_2 adsorption in IRMOFs in the temperature range of 40–120 K. The contribution values of the quantum effects were also calculated by Equation (2), and the $V_{\text{contribution}}$–loading curves were compared at different temperatures in three IRMOFs. Since the trends in each material studied here were similar, only the results in IRMOF-10 were shown in Figure 5 as an example. In addition, to discuss only the quantum effects resulting from temperature, the $V_{\text{contribution}}$ at each temperature in Figure 5 was presented as a function of loading instead of pressure. It can be seen from this figure that, under the same loading, the lower the temperature, the more evident are the quantum effects of H_2 adsorption. Moreover, the contributions of the quantum effects show a significant decreasing dependency on the adsorption loading at low temperature, while they become almost independent of the loading with temperature increasing.

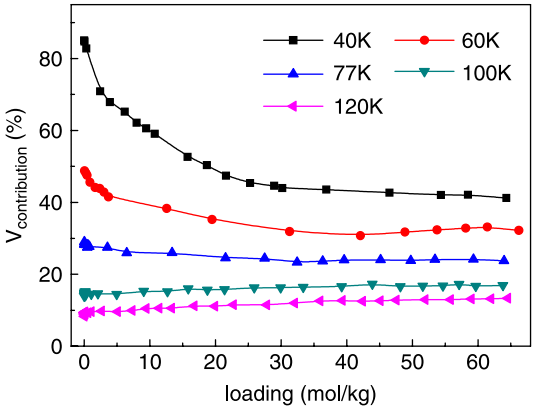

Figure 5. Comparison of the contribution values of quantum effects of H_2 adsorption in IRMOF-10 at different temperatures.

4. Conclusion

In conclusion, the influences of pore size and temperature on the quantum effects of H_2 adsorption in three IRMOFs were investigated by GCMC simulations with the quadratic FH effective potential. The simulation results show that the quantum effects of H_2 adsorption in IRMOF material with smaller pore size are more evident at low pressure (loading), while an opposite result appears with pressure (loading) increasing. In addition, this work also shows that the quantum effects are mainly contributed from the interactions between adsorbate and IRMOFs at low pressure (loading), and principally from the interactions between adsorbate molecules at high pressure (loading). Furthermore, the quantum effects become more evident as temperature decreases within the pressure range studied.

Acknowledgements

The financial support of the NSFC (Nos 20725622, 20706002, 20876006) is greatly appreciated.

References

[1] J.L.C. Rowsell and O.M. Yaghi, *Strategies for hydrogen storage in metal-organic frameworks*, Angew. Chem. Int. Ed. 44 (2005), pp. 4670–4679.
[2] R.Q. Snurr, J.T. Hupp, and S.T. Nguyen, *Prospects for nanoporous metal-organic materials in advanced separations processes*, AIChE J. 50 (2004), pp. 1090–1095.
[3] A.M. Seayad and D.M. Antonelli, *Recent advances in hydrogen storage in metal-containing inorganic nanostructures and related materials*, Adv. Mater. 16 (2004), pp. 765–777.
[4] J.L.C. Rowsell and O.M. Yaghi, *Metal-organic frameworks: A new class of porous materials*, Micropor. Mesopor. Mater. 73 (2004), pp. 3–14.
[5] M.J. Rosseinsky, *Recent developments in metal-organic framework chemistry: Design, discovery, permanent porosity and flexibility*, Micropor. Mesopor. Mater. 73 (2004), pp. 15–30.
[6] N.L. Rosi, J. Eckert, M. Eddaoudi, D.T. Vodak, J. Kim, M. O'Keeffe, and O.M. Yaghi, *Hydrogen storage in microporous metal-organic frameworks*, Science 300 (2003), pp. 1127–1129.
[7] B. Kesanli, Y. Cui, M.R. Smith, E.W. Bittner, B.C. Bockrath, and W. Lin, *Highly interpenetrated metal-organic frameworks for hydrogen storage*, Angew. Chem. Int. Ed. 44 (2005), pp. 72–75.
[8] Y. Kubota, M. Takata, R. Matsuda, R. Kitaura, S. Kitagawa, K. Kato, M. Sakata, and T.C. Kobayashi, *Direct observation of hydrogen molecules adsorbed onto a microporous coordination polymer*, Angew. Chem. Int. Ed. 44 (2005), pp. 920–923.
[9] D.N. Dybtsev, H. Chun, S.H. Yoon, D. Kim, and K. Kim, *Microporous manganese formate: A simple metal − organic porous material with high framework stability and highly selective gas sorption properties*, J. Am. Chem. Soc. 126 (2004), pp. 32–33.
[10] L. Pan, M.B. Sander, X. Huang, J. Li, M. Smith, E. Bittner, B. Bockrath, and J.K. Johnson, *Microporous metal organic materials: Promising candidates as sorbents for hydrogen storage*, J. Am. Chem. Soc. 126 (2004), pp. 1308–1309.
[11] J.L.C. Rowsell, A.R. Millward, K.S. Park, and O.M. Yaghi, *Hydrogen sorption in functionalized metal-organic frameworks*, J. Am. Chem. Soc. 126 (2004), pp. 5666–5667.
[12] F. Darkrim and D. Levesque, *Monte Carlo simulations of hydrogen adsorption in single-walled carbon nanotubes*, J. Chem. Phys. 109 (1998), pp. 4981–4984.
[13] Q. Wang and J.K. Johnson, *Hydrogen adsorption on graphite and in carbon slit pores from path integral simulations*, Mol. Phys. 95 (1998), pp. 299–309.

[14] Q. Wang, S.R. Challa, D.S. Sholl, and J.K. Johnson, *Quantum sieving in carbon nanotubes and zeolites*, Phys. Rev. Lett. 82 (1999), pp. 956–959.
[15] Q. Wang and J.K. Johnson, *Computer simulations of hydrogen adsorption on graphite nanofibers*, J. Phys. Chem. B 103 (1999), pp. 277–281.
[16] F. Darkrim, A. Aoufi, and D. Levesque, *Quantum contribution to gas adsorption in carbon nanotubes*, Mol. Simul. 24 (2000), pp. 51–61.
[17] S.R. Challa, D.S. Sholl, and J.K. Johnson, *Light isotope separation in carbon nanotubes through quantum molecular sieving*, Phys. Rev. B 63 (2001), pp. 1–9, 245419.
[18] C. Gu and G.H. Gao, *Path integral simulation of hydrogen adsorption in single-walled carbon nanotubes at low temperatures*, Phys. Chem. Chem. Phys. 4 (2002), pp. 4700–4708.
[19] H. Tanaka, M. El-Merraoui, T. Kodaira, and K. Kaneko, *Possibility of quantum effect in micropore filling of Ne on* $AlPO_4^{-5}$, Chem. Phys. Lett. 351 (2002), pp. 417–423.
[20] H. Tanaka, M. El-Merraoui, H. Kanoh, W.A. Steele, M. Yudasaka, S. Iijima, and K. Kaneko, *Quantum effects on hydrogen adsorption in internal nanospaces of single-wall carbon nanohorns*, J. Phys. Chem. B 108 (2004), pp. 17457–17465.
[21] H. Tanaka, J. Fan, H. Kanoh, Y. Yudasaka, S. Iijima, and K. Kaneko, *Quantum nature of adsorbed hydrogen on single-wall carbon nanohorns*, Mol. Simul. 31 (2005), pp. 465–474.
[22] H. Tanaka, H. Kanoh, M. Yudasaka, S. Iijima, and K. Kaneko, *Quantum effects on hydrogen isotope adsorption on single-wall carbon nanohorns*, J. Am. Chem. Soc. 127 (2005), pp. 7511–7516.
[23] P. Kowalczyk, H. Tanaka, R. Hołyst, K. Kaneko, T. Ohmori, and J. Miyamoto, *Storage of hydrogen at 303 K in graphite slitlike pores from grand canonical Monte Carlo simulation*, J. Phys. Chem. B 109 (2005), pp. 17174–17183.
[24] P. Kowalczyk, R. Hołyst, A.P. Terzyk, and P.A. Gauden, *State of hydrogen in idealized carbon slitlike nanopores at 77 K*, Langmuir 22 (2006), pp. 1970–1972.
[25] A.V.A. Kumar, H. Jobic, and S.K. Bhatia, *Quantum effects on adsorption and diffusion of hydrogen and deuterium in microporous*, J. Phys. Chem. B 110 (2006), pp. 16666–16671.
[26] P. Kowalczyk, P.A. Gauden, A.P. Terzyk, and S.K. Bhatia, *Thermodynamics of hydrogen adsorption in slit-like carbon nanopores at 77 K. Classical versus path-integral Monte Carlo simulations*, Langmuir 23 (2007), pp. 3666–3672.
[27] G. Garberoglio, A.I. Skoulidas, and J.K. Johnson, *Adsorption of gases in metal organic materials: Comparison of simulations and experiments*, J. Phys. Chem. B 109 (2005), pp. 13094–13103.
[28] G. Garberoglio, *Quantum sieving in organic frameworks*, Chem. Phys. Lett. (2008), Doi: 10.1016/j.cplett.2008.11.065.
[29] J.C. Liu, J.T. Culp, S. Natesakhawat, B.C. Bockrath, B. Zande, S.G. Sankar, G. Garberoglio, and J.K. Johnson, *Experimental and theoretical studies of gas adsorption in* $Cu_3(BTC)_2$*: An effective activation procedure*, J. Phys. Chem. C 111 (2007), pp. 9305–9313.
[30] J.C. Liu, J.Y. Lee, L. Pan, R.T. Obermyer, S. Simizu, B. Zande, J. Li, S.G. Sankar, and J.K. Johnson, *Adsorption and diffusion of hydrogen in a new metal-organic framework material:* $[Zn(bdc)(ted)_{0.5}]$, J. Phys. Chem. C 112 (2008), pp. 2911–2917.
[31] D. Noguchi, H. Tanaka, A. Kondo, H. Kajiro, H. Noguchi, T. Ohba, H. Kanoh, and K. Kaneko, *Quantum sieving effect of three-dimensional Cu-based organic framework for* H_2 *and* D_2, J. Am. Chem. Soc. 130 (2008), pp. 6367–6372.
[32] B. Chen, X. Zhao, A. Putkham, K. Hong, E.B. Lobkovsky, E.J. Hurtado, A.J. Fletcher, and K.M. Thomas, *Surface interactions and quantum kinetic molecular sieving for* H_2 *and* D_2 *adsorption on a mixed metal-organic framework material*, J. Am. Chem. Soc. 130 (2008), pp. 6411–6423.
[33] M. Eddaoudi, J. Kim, N. Rosi, D. Vodak, J. Wachter, M. O'Keefe, and O.M. Yaghi, *Systematic design of pore size and functionality in isoreticular MOFs and their application in methane storage*, Science 295 (2002), pp. 469–472.
[34] Accelrys, Inc., *Materials Studio*, 3.0V, Accelrys, Inc, San Diego, CA, 2003.
[35] T. Düren, F. Millange, G. Férey, K.S. Walton, and R.Q. Snurr, *Calculating geometric surface areas as a characterization tool for metal-organic frameworks*, J. Phys. Chem. C 111 (2007), pp. 15350–15356.
[36] D. Marx and P. Nielaba, *Path-integral Monte Carlo techniques for rotational motion in two dimensions: Quenched, annealed, and no-spin quantum-statistical averages*, Phys. Rev. A 45 (1992), pp. 8968–8971.
[37] Q. Yang and C. Zhong, *Electrostatic-field-induced enhancement of gas mixture separation in metal-organic frameworks: A computational study*, Chem. Phys. Chem. 7 (2006), pp. 1417–1421.
[38] Q. Yang and C. Zhong, *Molecular simulation of carbon dioxide/methane/hydrogen mixture adsorption in metal-organic frameworks*, J. Phys. Chem. B 110 (2006), pp. 17776–17783.
[39] A.K. Rappé, C.J. Casewit, K.S. Colwell, W.A. Goddard, III, and W.M. Skiff, *UFF, a full periodic table force field for molecular mechanics and molecular dynamics simulations*, J. Am. Chem. Soc. 114 (1992), pp. 10024–10035.
[40] R. Babarao, Z. Hu, J. Jiang, S. Chempath, and S.I. Sandler, *Storage and separation of* CO_2 *and* CH_4 *in silicalite, C168 schwarzite, and IRMOF-1: A comparative study from Monte Carlo simulation*, Langmuir 23 (2007), pp. 659–666.
[41] S. Keskin and D.S. Sholl, *Screening metal-organic framework materials for membrane-based methane/carbon dioxide separations*, J. Phys. Chem. C 111 (2007), pp. 14055–14059.
[42] B. Liu, Q.Y. Yang, C.Y. Xue, C.L. Zhong, B.H. Chen, and B. Smit, *Enhanced adsorption selectivity of hydrogen/methane mixtures in metal-organic frameworks with interpenetration: A molecular simulation study*, J. Phys. Chem. C 112 (2008), pp. 9854–9860.
[43] Q. Yang and C. Zhong, *Computational study of* CO_2 *storage in metal-organic frameworks*, J. Phys. Chem. C 112 (2008), pp. 1562–1569.
[44] L.M. Sesé, *Study of the Feynman–Hibbs effective potential against the path-integral formalism for Monte Carlo simulations of quantum many-body Lennard-Jones systems*, Mol. Phys. 81 (1994), pp. 1297–1312.
[45] L.M. Sesé, *Feynman–Hibbs potentials and path integrals for quantum Lennard-Jones systems: Theory and Monte Carlo simulations*, Mol. Phys. 85 (1995), pp. 931–947.
[46] D. Frenkel and B. Smit, *Understanding Molecular Simulation: From Algorithms to Applications*, Academic Press, San Diego, CA, 2002, pp. 126–130.
[47] B.A. Younglove, *Thermophysical properties of fluids. I. Argon, ethylene, parahydrogen, nitrogen, nitrogen trifluoride, and oxygen*, J. Phys. Chem. Ref. Data 11(Suppl. 1) (1982), pp. 1–356.
[48] N.A. Ramsahye, G. Maurin, S. Bourrelly, P.L. Llewellyn, C. Serre, T. Loiseau, T. Devic, and G. Ferey, *Probing the adsorption sites for* CO_2 *in metal organic frameworks materials MIL-53 (Al, Cr) and MIL-47 (V) by density functional theory*, J. Phys. Chem. C 112 (2008), pp. 514–520.
[49] K.S. Walton, A.R. Millward, D. Dubbeldam, H. Frost, J.J. Low, O.M. Yaghi, and R.Q. Snurr, *Understanding inflections and steps in carbon dioxide adsorption isotherms in metal-organic frameworks*, J. Am. Chem. Soc. 130 (2008), pp. 406–407.
[50] NIST, *NIST standard reference database number 69,* June 2005 Release, 2005, Available at http://webbook.nist.gov